Microgrooves and fluid flows provide preferential passageways for sperm over pathogen *Tritrichomonas foetus*

Chih-kuan Tung[a], Lian Hu[b,c], Alyssa G. Fiore[a], Florencia Ardon[b], Dillon G. Hickman[b], Robert O. Gilbert[d], Susan S. Suarez[b,1], and Mingming Wu[a,1]

Departments of [a]Biological and Environmental Engineering, [b]Biomedical Sciences, and [d]Clinical Sciences, Cornell University, Ithaca, NY 14853; and [c]Family Planning Research Institute, Center of Reproductive Medicine, Tongji Medical College, Huazhong University of Science and Technology, 430030 Wuhan, China

Edited by John J. Eppig, The Jackson Laboratory, Bar Harbor, ME, and approved March 13, 2015 (received for review January 9, 2015)

Successful mammalian reproduction requires that sperm migrate through a long and convoluted female reproductive tract before reaching oocytes. For many years, fertility studies have focused on biochemical and physiological requirements of sperm. Here we show that the biophysical environment of the female reproductive tract critically guides sperm migration, while at the same time preventing the invasion of sexually transmitted pathogens. Using a microfluidic model, we demonstrate that a gentle fluid flow and microgrooves, typically found in the female reproductive tract, synergistically facilitate bull sperm migration toward the site of fertilization. In contrast, a flagellated sexually transmitted bovine pathogen, *Tritrichomonas foetus*, is swept downstream under the same conditions. We attribute the differential ability of sperm and *T. foetus* to swim against flow to the distinct motility types of sperm and *T. foetus*; specifically, sperm swim using a posterior flagellum and are near-surface swimmers, whereas *T. foetus* swims primarily via three anterior flagella and demonstrates much lower attraction to surfaces. This work highlights the importance of biophysical cues within the female reproductive tract in the reproductive process and provides insight into coevolution of males and females to promote fertilization while suppressing infection. Furthermore, the results provide previously unidentified directions for the development of in vitro fertilization devices and contraceptives.

cell motility | cervix | microfluidics | microswimmer | trichomoniasis

For a successful fertilization, mammalian sperm must migrate through various compartments of the female reproductive tract to reach and fertilize oocytes. Human and bovine sperm, for example, must enter the cervix, swim against a gentle fluid flow, and pass through the uterus and narrow uterotubal junction into the oviduct before reaching the egg (Fig. 1*A*). It is now increasingly clear that biophysical cues within the female reproductive tract, including surface microgrooves (1, 2) and fluid flows (3, 4), critically regulate sperm cell migration. Microscopic examination of the bovine female reproductive tract show that longitudinally oriented microgrooves line the inner surfaces of the cervix and uterotubal junction (5, 6) (Fig. 1*A*). Many sperm were seen within microgrooves in histological sections of the bovine cervix (6). Furthermore, transmission electron micrographs of the bovine cervix showed that the beating of cilia lining the microgrooves is oriented toward the vagina, whereas the sperm are oriented in the opposite direction, indicating that sperm swim against currents created by ciliary beating in the grooves (6). In the human, scanning electron micrographs of the cervix indicate that longitudinal microgrooves are also present in the cervical lining (7). In mice, outward fluid flows have been observed in the oviduct and uterus (3). All together, previous work has provided strong evidence for the existence of fluid flow and micrometer-sized grooves in segments of the mammalian female reproductive tract. However, there is limited quantitative understanding about how fluid flows and microgrooves cooperatively regulate sperm migration, without concurrently facilitating the migration of pathogens.

Tritrichomonas foetus, a motile flagellate protozoan parasite, has a significantly negative economic impact on the cattle industry worldwide, particularly by reducing fertility (8, 9). In humans, a similar sexually transmitted pathogen, *Trichomonas vaginalis*, is reported by the World Health Organization to affect ~170 million people annually worldwide and is associated with preterm birth and low birth weight (10). Although extensive work has been carried out in learning how sperm swim upstream to ascend the female tract (4, 11), little is known about how pathogens gain access to upper regions of a female reproductive tract. In mammals, the female reproductive tract must protect itself against invasion by pathogens, yet facilitate passage of sperm to the site of fertilization (12). For humans, other primates, and cattle, the cervix is the primary filter that enables sperm passage but prevents the entry of pathogens. The uterotubal junction is another such filter and is the main filter for mammalian species in which males deposit sperm directly into the uterus.

Despite the increasingly recognized importance of the biophysical environment in mammal fertilization, there is limited understanding of how multiple biophysical factors within the female reproductive tract cooperatively facilitate sperm migration and at the same time reject sexually transmitted pathogens. In this study, we used a microfluidic device previously developed in our laboratories (2) to demonstrate that a gentle fluid flow,

Significance

Mammalian females must selectively allow sperm with normal morphology and motility to ascend the reproductive tract while rejecting invasion of pathogens. By using microfluidic modeling, we revealed that microgrooves and gentle fluid flows, two major biophysical characteristics of the female tract, synergistically provide preferential pathways for sperm. In contrast, the sexually transmitted pathogen, *Tritrichomonas foetus*, is swept away from these pathways. These findings are not only valuable to dairy and beef industries for maximizing fertility and suppressing disease, but also to human medicine, because the morphology and movement of bull sperm closely resemble those of human sperm, and *T. foetus* closely resembles *Trichomonas vaginalis*, which infects 170 million people annually worldwide.

Author contributions: S.S.S. and M.W. conceived the research project; C.K.T., L.H., F.A., R.O.G., S.S.S., and M.W. designed research; C.K.T., L.H., A.G.F., F.A., D.G.H., and R.O.G. performed research; C.K.T., L.H., A.G.F., F.A., and D.G.H. analyzed data; and C.K.T., L.H., F.A., R.O.G., S.S.S., and M.W. wrote the paper.

The authors declare no conflict of interest.

This article is a PNAS Direct Submission.

[1]To whom correspondence may be addressed. Email: mw272@cornell.edu or sss7@cornell.edu.

This article contains supporting information online at www.pnas.org/lookup/suppl/doi:10.1073/pnas.1500541112/-/DCSupplemental.

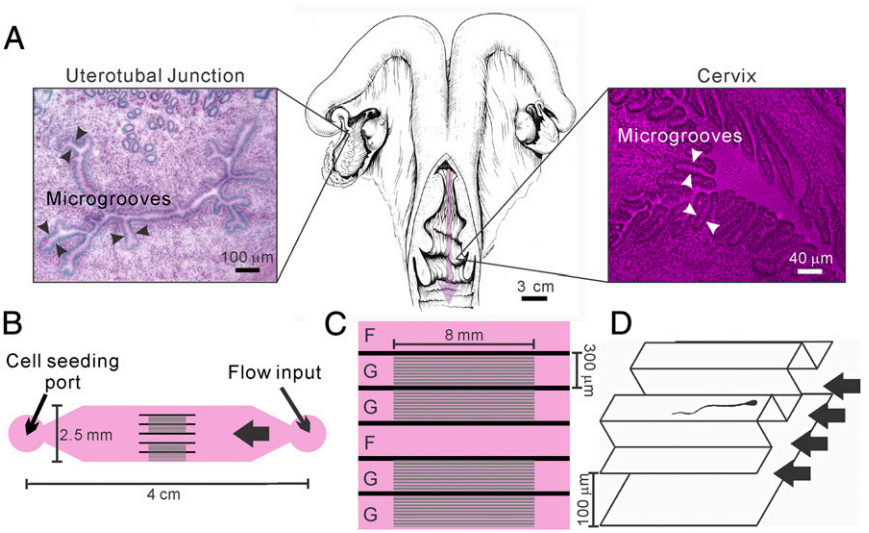

Fig. 1. A microfluidic device modeling fluid flows and microgrooves within the female reproductive tract. (*A*) Illustration (*Center*) of a bovine reproductive tract (adapted from ref. 36). The pink arrow points in the direction of fluid flow through the cervix. Microgrooves are seen in periodic acid-Schiff stain/hematoxylin-stained frozen sections of the uterotubal junction (*Left*) and the cervix (*Right*). Detailed methods are in ref. 5. (*B*) Illustration of the microfluidic device that recreates the microgrooves and the fluid flows that are in the female reproductive tract. Here, the cell seeding port is on one side and the flow inlet on the other, connected by channels with and without microgrooves. (*C*) Details of the channel design in the middle of the device. There are six channels for parallel experimentation; G denotes a channel with microgrooves in the upper surface, and F denotes a control channel lacking microgrooves. (*D*) A 3D drawing illustrates the details within a grooved channel. Here the main channel is 120 μm in height, and the microgrooves have a sectional area of 20 × 20 μm. Drawing is not to scale.

together with longitudinally oriented microgrooves on channel surfaces, synergistically facilitate sperm swimming upstream while sweeping a pathogen, *T. foetus*, downstream.

Results and Discussion

Microfluidic Model and Experimental Setup. A newly developed microfluidic model (Fig. 1*B*) was designed to simulate two important biophysical cues within the female reproductive tract: fluid flows and microgrooves embedded in the wall of the cervix and uterotubal junction (2). The microfluidic device consisted of a central channel 300 μm in width, 120 μm in height, and ∼4 cm in length. In the middle, the main channel was divided into six subchannels (as shown in Fig. 1*C*), of which the internal upper surfaces of four of the subchannels (labeled "G") were lined with microgrooves (Fig. 1*D*), mimicking the microgrooves in the cervix and uterotubal junction of cattle. The internal upper surfaces of the remaining channels (labeled "F") were smooth and served as controls. Each microgroove had a cross-sectional area of 20 × 20 μm. Cells were deposited at the "cell seeding port," and a gentle fluid flow was introduced in the "flow input" port via a syringe pump. Cells first swam away from the cell-seeding port and then encountered the grooved/smooth channels in the middle. Cell swimming behaviors were imaged by using high-speed digital video microscopy.

Differential Morphology, Motility, and Near-Surface Swimming Behavior of Sperm and *T. foetus*. We first examined the sperm and *T. foetus* swimming behavior when they swam on the smooth surface of the main channel in a low-viscosity aqueous medium [Tyrode albumin lactate pyruvate (TALP); ref. 13]. Bovine sperm have a paddle-shaped head (10 μm long, 5 μm wide, and 1 μm thick) and a single flagellum that is typically 50–60 μm long and 1 μm in diameter at the connection to the sperm head and then tapers to ∼200 nm in diameter at the distal end (Fig. 2*A*). The microscopic structures connecting the bovine sperm flagellum to the sperm head are slightly asymmetrically arranged along the thin dimension of the head (13, 14), and the broad surface of the head is flatter on one side than the other. The sperm moves by beating the posterior flagellum; this beating not only propels the sperm forward, but also induces rolling along the longitudinal axis [counter-clockwise (CCW) when viewed from in front of the sperm head] (ref. 15; Movie S1). At bovine body temperature (38.5 °C), the beat frequency of the flagellum was measured to be ∼20 Hz, and the rolling frequency of the entire cell body was ∼10 Hz. When introduced into the microfluidic device, sperm had the tendency to swim along channel surfaces or walls as discussed below. The sperm swimming trajectories on bottom surfaces were clockwise (CW) spirals when viewed from above, as seen in Fig. 2*A*. Sperm motility behaviors were robust, as little variability was seen across samples from three different bulls. We reported in a previous publication that the chiral trajectories are caused by the near-surface resistive force exerted on the sperm head (11). Chiral swimming trajectories are characteristics of all near-surface pusher microswimmers (16, 17). A pusher microswimmer exerts forces outward in the front and back of the cell. This class of swimmers, including sperm and *Escherichia coli*, are known to swim near surfaces in circular paths due to hydrodynamic interactions (16).

T. foetus, conversely, is a much less studied organism. It has three anterior flagella plus one so-called "recurrent" flagellum that arises anteriorly and is bent backward and secured periodically along the side of the cell body, creating an undulating membrane, before finally emerging at the posterior end of the cell as a freely moving tail (Fig. 2*B*). Its cell body is pear-shaped (18), and mature cells are 15 μm long and 7 μm wide (19). The three anterior flagella and the freely moving posterior flagellum are 12 ± 1 μm long (19). In contrast to sperm, *T. foetus* is much more rounded. In the TALP medium, the three anterior flagella orchestrated wave forms in the front of the *T. foetus* body and appeared to pull the cell forward (Movie S2). *T. foetus* is known to perform the eukaryotic version of run-and-tumble motion (19) (Fig. 2*B* and Movie S2) in a similar way as *Chlamydomonas reinhardtii* (20), which is a much-studied eukaryotic alga that swims by using two anterior flagella. *C. reinhardtii* runs when the flagella beat synchronously and tumbles when the flagella beat asynchronously (20–22). The tumbling results in a reorientation of the swimming direction. Given the similarities between the anterior flagella of *T. foetus* and *C. reinhardtii*, we will compare *T. foetus* to *C. reinhardtii* below.

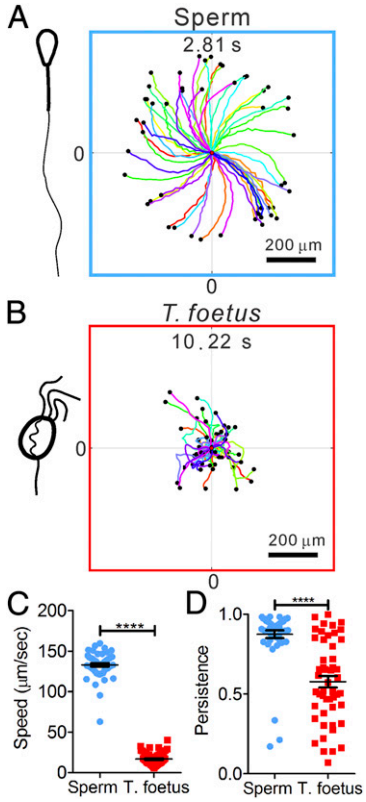

Fig. 2. Differential swimming behavior of bovine sperm and *T. foetus*. (*A* and *B*) Clockwise (CW) chiral trajectories of sperm (each 2.81 s long) (*A*) and random motion trajectories of *T. foetus* (each 10.22 s) (*B*). Each colored line is a swimming trajectory, and all of the trajectories start at (0,0) and end at the black dots. A total of 50 trajectories are shown in each plot. (*C*) Speeds of *T. foetus* are significantly slower than sperm. ****$P < 0.001$ (nonparametric Mann– Whitney test). (*D*) Sperm trajectories are more persistent than *T. foetus*. Persistence is defined as the ratio between the vector length of the displacement to the contour length of a trajectory. Error bars show SEM.

At bovine body temperature (38.5 °C), the sperm swam significantly faster and with higher directional persistence (vector length of the net displacement divided by the contour length of the trajectory) than *T. foetus* (Fig. 2*C*). Here the average sperm speed was 133 ± 2 μm/s, in contrast to 17 ± 1 μm/s for *T. foetus*. Sperm directional persistence was 0.87 ± 0.02, in contrast to 0.58 ± 0.04 for *T. foetus*.

The swimming patterns of sperm and *T. foetus* after they encountered vertical sidewalls of the microfluidic channels were found to be distinctly different. Fig. 3*A* shows that sperm tended to swim along the channel sidewalls once they hit the wall, whereas *T. foetus* either bounced off of the sidewalls immediately or swam along the walls for no more than 20 s until the next reorientation occurred—which was consistent with a previous report (Fig. 3*B*) (19). When examining the incoming and outgoing angles of short trajectories (~1.6 or 5.9 s), we found that outgoing angles of sperm were confined within 10° with respect to the sidewall, whereas the outgoing angles of *T. foetus* were essentially random (Fig. 3*D*). A few *T. foetus* stayed along the wall for a few seconds after the initial encounter.

These observations are consistent with our understanding that sperm are pusher microswimmers, like *E. coli* (23–25). When swimming close to a surface, the hydrodynamic interaction between the sperm and the surface attract the sperm toward the surface (26). In our microfluidic device, sperm were found to swim either along the upper or lower surface of the device as soon as they were introduced into the main channel (2). In contrast, the *T. foetus* exhibited swimming characteristics more in line with those of a puller microswimmer (20, 27) for the following reasons: (*i*) The wave motions of the *T. foetus* anterior flagella are similar to those of *C. reinhardtii* (19, 21), and (*ii*) both *T. foetus* and *C. reinhardtii*, like other puller microswimmers, do not have the tendency to swim near a surface (27). For *T. foetus*, we found that the majority of the organisms (61 ± 10%) bounced off of the sidewalls, but some of them remained swimming along sidewalls for a short period, typically for several seconds, and in rare cases for 10–20 s, as shown in Fig. 3*B*. This slight tendency to remain swimming along sidewalls is in contrast with *C. reinhardtii*, which immediately bounce off sidewalls at an angle that distributes with a narrow peak at 16° (27). Because bouncing off walls by puller microswimmers is determined by the beating configuration of the anterior flagella (27), the ability of *T. foetus* to move along the sidewall for a short time indicates that the recurrent flagellum—which forms an undulating membrane along the side of the cell body and a free swimming posterior portion—also plays a role in propulsion that is similar to pusher microswimmers, except when the cell tumbles to reorient (19). A recent report showed that the tumbling tendency of *E. coli* is suppressed when swimming near a solid surface (28). In *E. coli*, hydrodynamic interactions with walls prevent the unbundling of flagella, thereby inhibiting the tumbling. In contrast, *T. foetus* reorients by incoherent anterior flagella movements (19), and we clearly did not observe suppression of tumbling away from surfaces with *T. foetus*.

After encountering the microgrooves, sperm entered the microgrooves and swam within them, maintaining their initial swimming direction (Fig. 3*E*). In contrast, *T. foetus* did not tend to enter or swim within the microgrooves (Fig. 3*F*). As shown in Fig. 1*A*, the bovine cervix is lined with microgrooves on its internal surface, and many of the microgrooves have been found to maintain continuity through the length of the cervix (6). The attraction of sperm to surfaces in the device can be translated into their ability to enter and remain in the microfabricated grooves (Fig. 3*E*). Our findings indicate that the microgrooves in the cervix would provide strong guidance for sperm to migrate through the cervix into the uterus. These findings agree with electron-microscopy images, which show that many bull sperm are found in microgrooves in the cervix (6). In contrast, *T. foetus* did not stay in the microgrooves in the microfluidic devices or migrate along the microgrooves (Fig. 3*F*).

Sperm Swam Against a Gentle Flow, Whereas *T. foetus* Were Swept Away. Sperm and *T. foetus* responded to the presence of fluid flow very differently. In Fig. 4 *A–C*, we show that sperm swam actively against the flow when the flow exceeded a critical rate (11), whereas *T. foetus* were passively swept away (also see Movie S3). At low flow rates, <1 μL/min, sperm maintained their chiral trajectories in all directions. When the flow was increased above the threshold rate to ~2 μL/min, sperm oriented into the flow and swam upstream, whereas *T. foetus* were swept downstream. Interestingly, Fig. 4*C* shows that *T. foetus* were brought downstream by a flow of only 1 μL/min, which had no significant effect on sperm. In fact, no upstream swimming was observed for *T. foetus*, even when the flow rate was lowered to ~0.05 μL/min, which is ~5% of the critical flow rate for the onset of sperm upstream swimming.

The roles of fluid flows in guiding sperm migration have been reported recently by us (11), as well as other investigators (3, 4). Our work demonstrated that sperm upstream swimming is governed by near-surface hydrodynamic interaction, via the interactions of a front–back asymmetric microswimmer with a solid boundary. Therefore, when sperm are far away from a solid surface, there will be no force that orients them upstream (11). Moreover, the upstream swimming is governed by hydrodynamic bifurcation theory, which applies to a broad class of microswimmers that swim close to a surface and in a chiral trajectory (11). In contrast, *T. foetus* exhibit swimming behaviors that are distinctly different from those of sperm. They do not swim near a surface, and their front-to-back asymmetry is less pronounced than that of sperm,

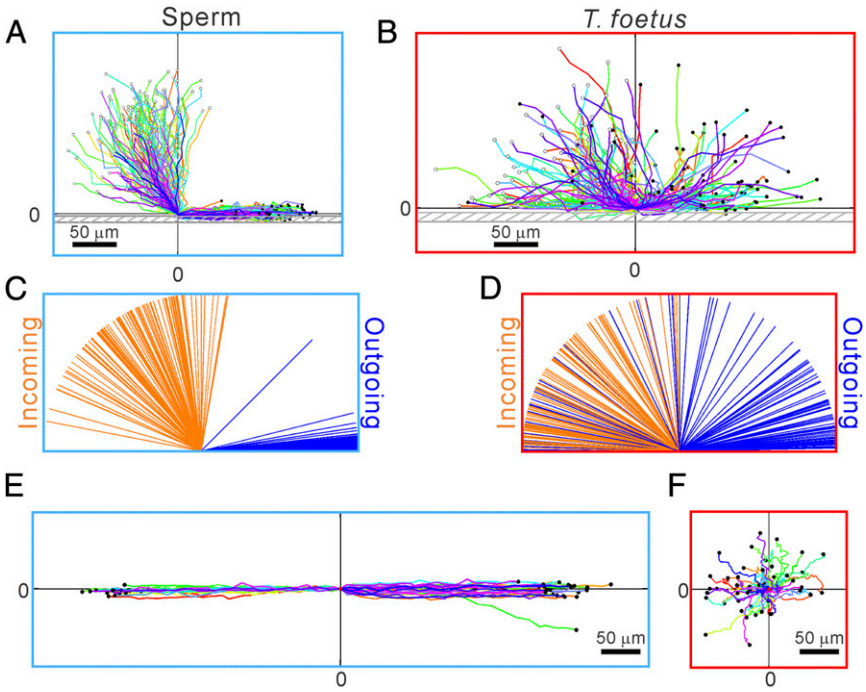

Fig. 3. Differential swimming behavior of sperm and *T. foetus* near a channel side wall. (*A* and *B*) Trajectories of sperm (*A*) and *T. foetus* (*B*) when they encounter a sidewall. Here, (0,0) is defined as the center position of the cell head at the time when the cell head hits the wall, and the wall is parallel to the *x* axis. Most sperm swim parallel to the wall after hitting it; in contrast, most *T. foetus* leave the wall in a random direction, whereas some of them swim along the wall for a few seconds before leaving the wall. Each trajectory is ∼1.6 s (*A*) or 5.9 s (*B*) long. (*C* and *D*) Line diagram showing the incoming and outgoing angles of the sperm (*C*) and *T. foetus* (*D*) before and after they hit a sidewall. Cell locations 0.4 s (*C*) or 1.48 s (*D*) away from (0,0) were used to calculate the angles. $n = 100$. (*E* and *F*) Swimming trajectories of sperm (*E*) and *T. foetus* (*F*) near a surface patterned with microgrooves. When sperm encountered the microgrooves, they entered and followed the grooves. When *T. foetus* encountered the grooves, they did not swim into the grooves; instead, they executed random motion in all directions. $n = 50$.

which yields less hydrodynamic coupling for *T. foetus* (11, 29). Because the upstream swimming bias of sperm requires sperm to interact hydrodynamically with a surface (11) and *T. foetus* exhibit very low attraction to surfaces, *T. foetus* cannot be oriented upstream by a flow or take advantage of the reduced flow provided by a no-slip boundary close to a surface. It is therefore conceivable that limited attraction to surfaces is what renders *T. foetus* so susceptible to being swept away by fluid flow.

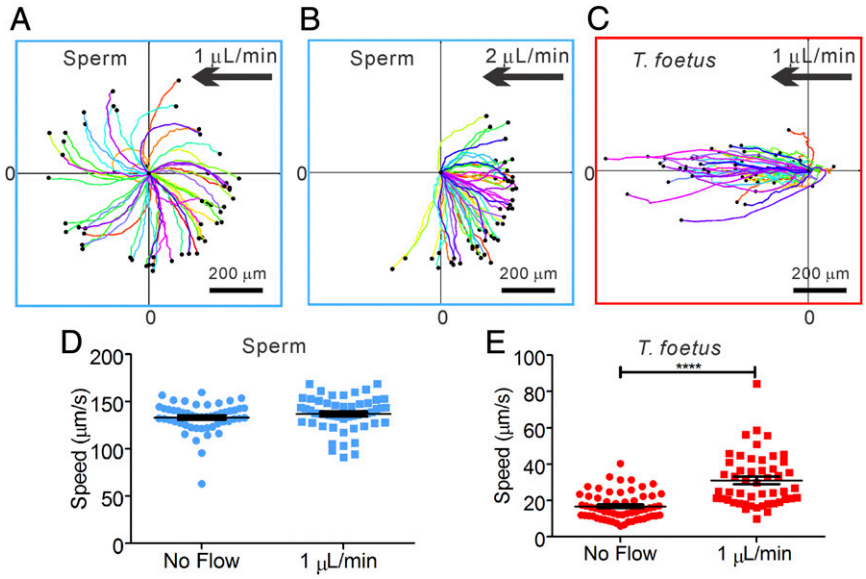

Fig. 4. Sperm swim upstream and *T. foetus* are swept away by a gentle flow. (*A*) At 1 μL/min flow, sperm trajectories are similar to the case in which there is no flow. (*B*) At 2 μL/min flow, sperm swim against the flow. (*C*) Almost all (but one) *T. foetus* are swept downstream by a 1 μL/min flow. (*D*) A gentle flow of 1 μL/min has very limited impact on the motility of sperm, because the difference in speeds is not statistically significant ($P = 0.25$). (*E*) Motility of *T. foetus* is significantly altered by the presence of a flow. The higher speed in the presence of the flow is due to the fact that *T. foetus* were passively swept away by the flow. Flow speed in the channel has a Poiseuille profile across the vertical direction and ranges from 6 to 86 μm/s. *T. foetus* is distributed along the vertical direction in the channel. Number of cells analyzed is 50. Error bars show SEM.

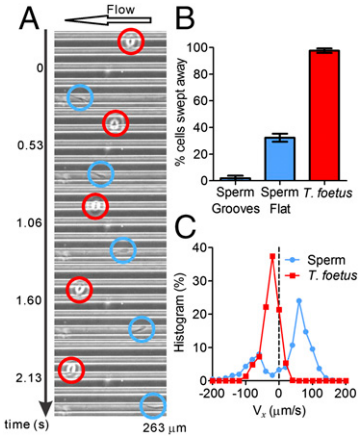

Fig. 5. Microgrooves facilitate upstream swimming in sperm, but have no impact on *T. foetus*. (*A*) A montage of micrographs shows sperm (blue circles) swimming against the flow in a microgroove, whereas a *T. foetus* (red circles) does not enter the microgroove and is brought downstream. (*B*) Percentage of cells swept away by a 3 μL/min flow in three different situations: sperm swimming within microgrooves, sperm on a flat surface, and *T. foetus* on a flat surface. $n = 50$. Error bars show SEM. (*C*) Histogram of instantaneous x-velocity shows an upstream bias for sperm at a 3 μL/min flow and a downstream bias for *T. foetus* at 1 μL/min flow. Statistics were acquired from 50 tracks of sperm (2.81 s long) and 50 tracks of *T. foetus* (10.22 s long).

Our experimental flow rates were determined empirically; that is, we started at the lowest setting of the pump and increased it until sperm responded by orienting into the current. Then we increased the flow rate in steps until most sperm were swept away by the current. The flow rate at which the sperm started to reorient was 1.13 ± 0.06 μL/min, or 15.1 ± 0.8 μm/s at a plane 5 μm above the bottom surface of the channel, in agreement with our previous findings (11). Currently, no reports are available on rates of fluid flow in the bovine reproductive tract; however, in mice, similar flow rates of 18 ± 2 μm/s were measured in the oviduct after mating (3). In vivo, fluid flow is caused by combinations of ciliary action, muscle contraction, and secretion, which change with hormonal conditions and mating (3).

Microgrooves and Fluid Flows Cooperatively Provide Preferential Migration Pathways for Sperm over *T. foetus*. When subject to both a gentle flow and microgrooves, sperm quickly gained access to the microgrooves and swam upstream efficiently, whereas *T. foetus* did not enter the microgrooves and were swept downstream by the flow (Fig. 5*A* and Movie S4). Fig. 5*B* shows that almost all (99%) *T. foetus*, but only 2% of sperm, were swept away close to the grooved surfaces in the presence of a flow of 3 μL/min. In the case of smooth surfaces, 32% of sperm were swept away using the same flow rate of 3 μL/min. If we examine the distribution of instantaneous velocity parallel to the flow direction (x component), sperm were overwhelmingly found to move against the flow, and *T. foetus* was found to move with the flow (Fig. 5*C*). The different responses of sperm and *T. foetus* demonstrate that fluid flows and microgrooves on channel surfaces cooperatively facilitate sperm upstream swimming, whereas microgrooves have no impact on *T. foetus* migration, and fluid flows sweep *T. foetus* downstream.

Viscoelastic Medium Did Not Change the Basic Swimming Behaviors of Sperm and *T. foetus*. Because fluids in the bovine cervix and oviduct contain secreted mucus, which increases fluid viscoelasticity, we further studied the swimming behavior of sperm and *T. foetus* in viscoelastic fluids. A 0.7% long-chain polyacrylamide (PAM) solution dissolved in TALP medium was used to model estrous bovine cervical mucus, because the loss modulus of 0.7% PAM is similar to that of estrous bovine cervical mucus (Fig. S1), and sperm swam in the PAM solution in a way similar to when they swam in cervical mucus (Movies S5 and S6). In contrast to their swimming behavior in low-viscoelasticity medium, sperm in high-viscoelasticity medium swam without rolling (Movie S5), moved more slowly, and followed CCW (viewed from above) chiral trajectories (Fig. 6 *A* and *B*). Nevertheless, sperm in high-viscoelasticity medium retained the key features of pusher swimmers, in that they continued to exhibit attraction to surfaces and produced chiral trajectories on flat surfaces, as shown in Fig. 6 *A* and *C*. The swimming behaviors of *T. foetus* were very similar in low- and high-viscoelasticity media (Movie S7) and showed no evidence of strong attraction to surfaces. Based on the above analysis and our understanding of near-surface microswimmers (11), we conclude that the microgrooves on surfaces and fluid flows provide a preferential pathway for sperm over *T. foetus* to swim upstream in viscoelastic fluids, such as those present in the female tract.

Conclusions

Our results demonstrate that microgrooves in the wall of the mammalian female reproductive tract and a gentle outward flow within the tract can cooperatively act to facilitate migration of sperm toward the site of fertilization while preventing invasion of pathogens. Using our in vitro microfluidic model, we have provided evidence that aspects of mammalian sperm and *T. foetus* morphology dictate swimming behaviors in response to walls and flows. Our results suggest that sperm morphology could have coevolved with the development of microgrooves in the walls of the female tract. Strong evidence has been reported for coevolution of morphologies of male gametes and female reproductive tracts in insects (30). Infections of *T. foetus* and *T. vaginalis* sometimes do ascend the female tract; however, the mechanism of ascent is currently unknown and may not depend on flagellum-based swimming. Trichomonads transform into an amoeboid form when they infect vaginal epithelium (31); however, it is not known whether this form is used to ascend the tract. Because migrating to the upper female tract does not enable trichomonads to spread to other hosts, it is reasonable to conclude that there is little selection pressure for them to evolve the ability for upstream swimming along microgrooves.

In conclusion, this work advances our understanding of how the female reproductive tract facilitates sperm migration to the fertilization site while suppressing pathogen migration. We have

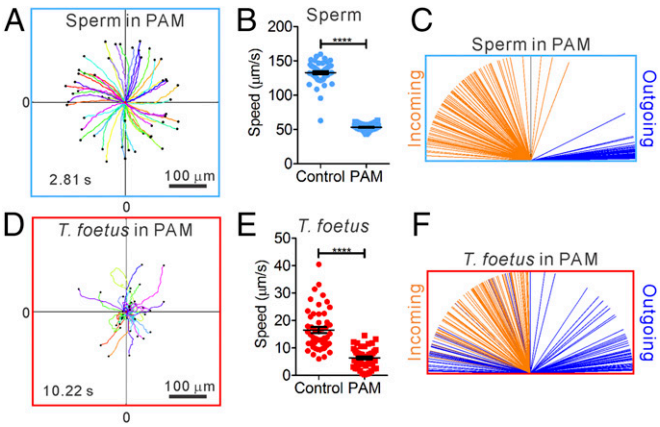

Fig. 6. Swimming behaviors of sperm and *T. foetus* in viscoelastic fluid. (*A*) CCW chiral trajectories of swimming sperm. (*B*) Sperm swim significantly slower in the presence of PAM than in control medium. $n = 50$. (*C*) Sperm swim along a wall after it hits the wall in the presence of PAM. $n = 100$. (*D*) Random motion of *T. foetus* in the presence of PAM. (*E*) *T. foetus* swim significantly slower in the presence of PAM than in control medium. $n = 50$. Error bars show SEM. (*F*) *T. foetus* does not show a tendency to swim along the wall after it hits the wall. $n = 100$.

focused here on two physical aspects of the interactions of sperm and trichomonads with the female tract. In future work, these physical interactions should be examined in combination with molecular interactions between sperm, trichomonads, and the epithelial lining of the female reproductive tract to understand more fully how these organisms move through the tract and how the female regulates their movements. The knowledge derived can be used to improve contraception and protection against sexually transmitted diseases, as well as to develop new technology for selection of sperm for in vitro fertilization and for assessment of fertility of sperm samples.

Materials and Methods

Bull Sperm Samples. Experiments were performed independently with semen from three different fertile bulls. Bull semen samples frozen in 250-μL plastic commercial artificial insemination straws were generously provided by Genex Cooperative (Ithaca, NY). Frozen straws were first thawed in a 37 °C water bath, and then seminal plasma, cryopreservation diluent, abnormal sperm, and dead sperm were removed from live sperm by density gradient centrifugation (300 × *g* for 10 min) through two layers (40–80%) of BoviPure diluted in BoviDilute, according to the manufacturer's recommendations (Nidacon International) (32). The sperm pellet was then washed in 3 mL of TALP (300 × *g* for 5 min) (33). Sperm were resuspended in ∼20 μL of TALP medium. After processing, >85% of the sperm had normal morphology and motility.

***T. foetus* Samples.** *T. foetus* were purchased from Biomed Diagnostics. The initial live cultures and their subcultures were maintained in InPouch TF Bovine plastic pouches containing a proprietary medium selective for TF growth. InPouch TF is widely used in the United States for bovine trichomoniasis diagnosis (34, 35). *T. foetus* were subcultured every 3–4 d by using fresh pouches. Experiments were performed with three different subcultures on the second day after each subculture had been prepared. *T. foetus* were first centrifuged for 6 min at 300 × *g* and then resuspended into 50–100 μL of *T. foetus* medium (depending on cell density) for seeding into the microfluidic devices.

Microfluidic Assays. Devices were made of polydimethylsiloxane, using standard stamping techniques, with a two-layer etched silicon wafer treated with (1H,1H,2H,2H-perfluorooctyl) trichlorosilane. Before the experiments, channels were filled with TALP (to be used as control) or 0.7% long-chain PAM (Scientific Polymer Products; molecular mass 5–6 MDa) dissolved in TALP and equilibrated overnight with 5% CO_2 in humidified air at 38.5 °C (bovine core body temperature). For the experiments, the microfluidic devices were placed on a temperature-controlled glass plate (OkoLab) on a heated microscope stage (Carl Zeiss), which was kept at 38.5 °C. Sperm were seeded into one end of the device, and then medium was pumped in at the opposite end. Different flow rates were then applied by a syringe pump (KD Scientific). We waited 1 min for the flow to stabilize before commencing imaging for each flow rate (2).

Cell Imaging and Analysis. Images of sperm were acquired at 17.8–19.55 frames per s (FPS) by using phase-contrast microscopy (10× objective) by a Neo sCMOS high-speed digital camera (Andor) and the NIS Elements imaging software (Version 4.0; Nikon). To analyze the sperm movement in the digital video recordings, the locations of sperm heads were tracked manually from image to image by using ImageJ and MATLAB.

Rheology Measurements. Dynamic moduli were measured by using a rotational shear rheometer (TA Instruments; DHR3) with a 25-mm stainless steel parallel plate at 38.5 °C, running in oscillation mode. Maximum strain was 0.1%. Bovine cervical mucus samples were obtained from lactating Holstein cows in spontaneous estrus. Increased activity of cows was identified by Alpro activity monitors, with data processed using the Alpro Herd Management System [Alpro for Windows (Version 7.1); DeLaval]. Behavioral estrus was then confirmed visually. The cows were restrained and their perineum cleansed, and a sterile plastic infusion pipette was inserted to the cranial vagina under transrectal palpation control. Mucus was aspirated by using a 30-mL syringe. Measurement was conducted within 1 h after the sample collection.

ACKNOWLEDGMENTS. We thank M. Wolfner for helpful discussion. This work was supported primarily by the National Institutes of Health (1R01HD070038 to S.S.S. and M.W.), and partially by the US Department of Agriculture, National Institute of Food and Agriculture (Hatch grant to M.W.). This work made use of the Cornell Center for Materials Research Shared Facilities which are supported through the National Science Foundation Materials Research Science and Engineering Centers program (DMR-1120296), the Cornell NanoScale Science & Technology Facility, and the Cornell Nanobiotechnology Center.

1. Denissenko P, Kantsler V, Smith DJ, Kirkman-Brown J (2012) Human spermatozoa migration in microchannels reveals boundary-following navigation. *Proc Natl Acad Sci USA* 109(21):8007–8010.
2. Tung C-K, Ardon F, Fiore AG, Suarez SS, Wu M (2014) Cooperative roles of biological flow and surface topography in guiding sperm migration revealed by a microfluidic model. *Lab Chip* 14(7):1348–1356.
3. Miki K, Clapham DE (2013) Rheotaxis guides mammalian sperm. *Curr Biol* 23(6): 443–452.
4. Kantsler V, Dunkel J, Blayney M, Goldstein RE (2014) Rheotaxis facilitates upstream navigation of mammalian sperm cells. *eLife* 3:e02403.
5. Suarez SS, Brockman K, Lefebvre R (1997) Distribution of mucus and sperm in bovine oviducts after artificial insemination: The physical environment of the oviductal sperm reservoir. *Biol Reprod* 56(2):447–453.
6. Mullins KJ, Saacke RG (1989) Study of the functional anatomy of bovine cervical mucosa with special reference to mucus secretion and sperm transport. *Anat Rec* 225(2):106–117.
7. Kessel RG (1979) *Tissues and Organs: A Text-Atlas of Scanning Electron Microscopy* (Freeman, San Francisco).
8. Bondurant RH (2005) Venereal diseases of cattle: Natural history, diagnosis, and the role of vaccines in their control. *Vet Clin North Am Food Anim Pract* 21(2):383–408.
9. Jin Y, Schumaker B, Logan J, Yao C (2014) Risk factors associated with bovine trichomoniasis in beef cattle identified by a questionnaire. *J Med Microbiol* 63(Pt 6):896–902.
10. Carlton JM, et al. (2007) Draft genome sequence of the sexually transmitted pathogen Trichomonas vaginalis. *Science* 315(5809):207–212.
11. Tung C-K, et al. (2015) Emergence of upstream swimming via a hydrodynamic transition. *Phys Rev Lett* 114(10):108102.
12. Mattner PE (1968) The distribution of spermatozoa and leucocytes in the female genital tract in goats and cattle. *J Reprod Fertil* 17(2):253–261.
13. Ho H-C, Suarez SS (2003) Characterization of the intracellular calcium store at the base of the sperm flagellum that regulates hyperactivated motility. *Biol Reprod* 68(5):1590–1596.
14. Ounjai P, Kim KD, Lishko PV, Downing KH (2012) Three-dimensional structure of the bovine sperm connecting piece revealed by electron cryotomography. *Biol Reprod* 87(3):73.
15. Gaffney EA, Gadêlha H, Smith DJ, Blake JR, Kirkman-Brown JC (2011) Mammalian sperm motility: Observation and theory. *Annu Rev Fluid Mech* 43(1):501–528.
16. Lauga E, DiLuzio WR, Whitesides GM, Stone HA (2006) Swimming in circles: Motion of bacteria near solid boundaries. *Biophys J* 90(2):400–412.
17. Su T-W, Xue L, Ozcan A (2012) High-throughput lensfree 3D tracking of human sperms reveals rare statistics of helical trajectories. *Proc Natl Acad Sci USA* 109(40):16018–16022.
18. Benchimol M (2004) Trichomonads under microscopy. *Microsc Microanal* 10(5): 528–550.
19. Lenaghan SC, Nwandu-Vincent S, Reese BE, Zhang M (2014) Unlocking the secrets of multi-flagellated propulsion: Drawing insights from *Tritrichomonas foetus*. *J R Soc Interface* 11(93):20131149.
20. Polin M, Tuval I, Drescher K, Gollub JP, Goldstein RE (2009) Chlamydomonas swims with two "gears" in a eukaryotic version of run-and-tumble locomotion. *Science* 325(5939):487–490.
21. Goldstein RE, Polin M, Tuval I (2009) Noise and synchronization in pairs of beating eukaryotic flagella. *Phys Rev Lett* 103(16):168103.
22. Bennett RR, Golestanian R (2013) Emergent run-and-tumble behavior in a simple model of Chlamydomonas with intrinsic noise. *Phys Rev Lett* 110(14):148102.
23. Berke AP, Turner L, Berg HC, Lauga E (2008) Hydrodynamic attraction of swimming microorganisms by surfaces. *Phys Rev Lett* 101(3):038102.
24. Li G, Tang JX (2009) Accumulation of microswimmers near a surface mediated by collision and rotational Brownian motion. *Phys Rev Lett* 103(7):078101.
25. Drescher K, Dunkel J, Cisneros LH, Ganguly S, Goldstein RE (2011) Fluid dynamics and noise in bacterial cell-cell and cell-surface scattering. *Proc Natl Acad Sci USA* 108(27):10940–10945.
26. Rothschild (1963) Non-random distribution of bull spermatozoa in a drop of sperm suspension. *Nature* 198(488):1221.
27. Kantsler V, Dunkel J, Polin M, Goldstein RE (2013) Ciliary contact interactions dominate surface scattering of swimming eukaryotes. *Proc Natl Acad Sci USA* 110(4):1187–1192.
28. Molaei M, Barry M, Stocker R, Sheng J (2014) Failed escape: Solid surfaces prevent tumbling of *Escherichia coli*. *Phys Rev Lett* 113(6):068103.
29. Brotto T, Caussin J-B, Lauga E, Bartolo D (2013) Hydrodynamics of confined active fluids. *Phys Rev Lett* 110(3):038101.
30. Higginson DM, Miller KB, Segraves KA, Pitnick S (2012) Female reproductive tract form drives the evolution of complex sperm morphology. *Proc Natl Acad Sci USA* 109(12):4538–4543.
31. Kusdian G, Woehle C, Martin WF, Gould SB (2013) The actin-based machinery of *Trichomonas vaginalis* mediates flagellate-amoeboid transition and migration across host tissue. *Cell Microbiol* 15(10):1707–1721.
32. Ardon F, Suarez SS (2013) Cryopreservation increases coating of bull sperm by seminal plasma binder of sperm proteins BSP1, BSP3, and BSP5. *Reproduction* 146(2):111–117.
33. Parrish JJ, Susko-Parrish J, Winer MA, First NL (1988) Capacitation of bovine sperm by heparin. *Biol Reprod* 38(5):1171–1180.
34. Schönmann MJ, et al. (1994) Comparison of sampling and culture methods for the diagnosis of *Tritrichomonas foetus* infection in bulls. *Vet Rec* 134(24):620–622.
35. Cobo ER, et al. (2007) Sensitivity and specificity of culture and PCR of smegma samples of bulls experimentally infected with *Tritrichomonas foetus*. *Theriogenology* 68(6):853–860.
36. Roberts SJ (1986) *Veterinary Obstetrics and Genital Diseases (Theriogenology)* (David and Charles, Woodstock, VT), 3rd Ed.